A 2D ray-based maximum field Green's function simulator

Paulo E. M. Cunha PETROBRAS S/A

Abstract

Going against last decade's hegemonic trend to propagate the field through the wave front reconstruction (Lambaré et al., 1996), this method is based on the full tracing of each ray at a time and the immediate application of information available in Hamilton's differential equations (1) and the first variation (2) thereof. After that, all information of the ray is discarded avoiding to spend great amount of RAM memory.

The algorithm is even capable to capture the maximum field times and amplitudes aiming to increment the seismic imaging quality.

Thus, like all others, it does not represent any structural reformulation in the ray theory (Popov, 1977), (Popov and Pšenčik, 1978b), (Popov and Pšenčik, 1978a), but rather the details in the form of its implementation to obtain a higher effectiveness for industrial purposes.

It is different from other similar methods also based on the full ray tracing by and efficient precision control, by having a criterion consistent with geometric optics and asymptotic series.

The heart of the algorithm is the way to extrapolate amplitudes from an ray point to an grid point.

It is robust and can be employed both in seismic imaging and in velocity field inversion by travel time tomography.

The proposed algorithm involves the numerical asymptotic solution of the extended (include the second derivative of slowness respect to the ray parameter) differential equations system, in rectangular coordinates, followed by the determination Taylor's series coefficients and the expansion around one region close to each ray point.

Despite the need to solve a system of ODEs the algorithm allows to avoid to propagate field in shadow zone, in this case it can achieve a orders of magnitude faster than Eikonal solvers like Schneider's.

Introduction

The recent advances in the intensive computational technology with production of high computational capacity machines, particularly the parallel architectures, have woken up crescent attention to the seismic depth imaging which is highly sensitive to the velocity field errors.

The velocity field analysis and travel time tomography demands fast and accurate algorithms.

The main motivation for using reverse time migration (RTM) is to employ the full acoustical - elastic wave equation to propagate the stress field, where it is implicit the presence of a punctual Green's function centered in the source - receptor stations, which makes the implementation of the maximum field travel time (MFT) natural and simple.

The experience with real data indicates that the RTM results for complex media are sometimes superior than that obtained by other methods (sometimes worst than time migration). We believe that part of this qualitative superiority could be credited just to the MFT, as supported by this work.

This work presents the results of building the maximum field travel times and amplitudes by the solution of the kinematic and dynamical ray tracing system of differential equations.

This corresponds to include the field amplitude propagation in the version already developed (Cunha, 2003), with adaptive step time control between the ray points (Cunha, 1999).

Between several velocity models the *SEG/EAGE* (Aminzadeh et al., 1997) was purposefully chosen as a hard test since it naturally infringes some of the basic assumptions for the good performance of asymptotic methods such as high frequencies and / or certain degree of smoothness of the velocity field. The image condition for a point source was determined like RTM, by the Finite Difference Method (FDM), which gives the reference maximum field travel times (MFT) and amplitudes (MFA) to compare with the results obtained by the proposed method.

Theory

The algorithm is based on the solution of the system of the kinematic differential equations:

$$\frac{d}{d\sigma}\begin{bmatrix}\boldsymbol{x}(\sigma)\\ \boldsymbol{p}(\sigma)\end{bmatrix} = J\begin{bmatrix}-\nabla_{\boldsymbol{x}}\left(\frac{1}{2c^2(\boldsymbol{x}(\sigma))}\right)\\ \boldsymbol{p}\end{bmatrix}, \qquad (1)$$

and dynamic,

$$\frac{d}{d\sigma}\begin{bmatrix}\frac{\partial \boldsymbol{x}}{\partial \gamma}(\sigma)\\ \frac{\partial \boldsymbol{p}}{\partial \gamma}(\sigma)\end{bmatrix} = J\begin{bmatrix}-\nabla_{\boldsymbol{x}}\nabla_{\boldsymbol{x}}\left(\frac{1}{2c^2(\boldsymbol{x}(\sigma))}\right) & \mathbf{0}\\ \mathbf{0} & \mathbf{1}\end{bmatrix}\begin{bmatrix}\frac{\partial \boldsymbol{x}}{\partial \gamma}(\sigma)\\ \frac{\partial \boldsymbol{p}}{\partial \gamma}(\sigma)\end{bmatrix}. \qquad (2)$$

The first system of equations (1) provides the trajectory $x(\sigma)$ and the slowness $\boldsymbol{p}(\boldsymbol{x}(\sigma))$ of the rays, where σ is a parameter defined by the equations (3), $d\tau$ is the time interval, ds is the interval of the arc length, $c(x(\sigma))$ is the velocity field and $\gamma = \{\sigma, \alpha\}$ the 2D global ray coordinates α as the takeoff angle.

$$J = \begin{bmatrix}\mathbf{0} & \mathbf{1}\\ -\mathbf{1} & \mathbf{0}\end{bmatrix}, \quad d\sigma = c\,ds = c^2 d\tau, \quad \boldsymbol{p} = \frac{\boldsymbol{t}}{c} = \nabla_{\boldsymbol{x}}\tau, \qquad (3)$$

Lets define: $\boldsymbol{x}_0 \equiv \boldsymbol{x}(\sigma_0, \gamma_0)$, $\boldsymbol{x} \equiv \boldsymbol{x}(\sigma, \gamma)$, $\boldsymbol{p}_0 \equiv \boldsymbol{x}(\sigma_0, \gamma_0)$ and $\boldsymbol{p} \equiv \boldsymbol{x}(\sigma, \gamma)$ the vectors in rectangular coordinates of

the ray and grid points, ray and grid slowness respectively. Then:

$$\delta\boldsymbol{x} = \boldsymbol{x} - \boldsymbol{x}_0\ , \qquad \delta\boldsymbol{p} = \boldsymbol{p} - \boldsymbol{p}_0\ , \tag{4}$$

$$\delta\boldsymbol{x}(\sigma) = \frac{\partial\boldsymbol{x}(\sigma)}{\partial\boldsymbol{\gamma}}\ \delta\boldsymbol{\gamma}\ , \qquad \delta\boldsymbol{p}(\sigma) = \frac{\partial\boldsymbol{p}(\sigma)}{\partial\boldsymbol{\gamma}}\ \delta\boldsymbol{\gamma}\ , \tag{5}$$

are respectively the variations of the vectors position and slowness with respect to the central ray.

Travel time extrapolation

The extrapolation of the travel transit times $\tau_0 \equiv \tau(\boldsymbol{x}_0)$ of the points of the ray for the travel times $\tau \equiv \tau(\boldsymbol{x})$ in the points of the grid is made through the expansion of the Taylor series, for the maximum field travel times, to the second order term, that is:

$$\tau(\boldsymbol{x}) = \tau(\boldsymbol{x}_0) + \boldsymbol{p}(\boldsymbol{x}_0)\cdot\delta\boldsymbol{x} + \frac{1}{2}\langle\langle M_0, \delta\boldsymbol{x}\rangle,\ \delta\boldsymbol{x}\rangle + \mathcal{O}(|\delta\boldsymbol{x}|^3)\ . \tag{6}$$

where $\langle\ ,\ \rangle$ is the dot product and matrix M_0 equation (7) is the second order contribution to the Taylor series,

$$M_0 = \left[\frac{\partial\boldsymbol{p}}{\partial\boldsymbol{\gamma}}\right]\left[\frac{\partial\boldsymbol{x}}{\partial\boldsymbol{\gamma}}\right]^{-1}\Bigg|_{\boldsymbol{x}_0}, \qquad {}^{\sigma}\mathcal{J} = \det\left[\frac{\partial\boldsymbol{x}}{\partial\boldsymbol{\gamma}}\right]\Bigg|_{\boldsymbol{x}_0} > \epsilon\ , \tag{7}$$

The Taylor series will be expanded only out of caustics by satisfying the second equation of (7). The slowness $\boldsymbol{p}(\boldsymbol{x}_0)$ and ray coordinates $\boldsymbol{x}_0$ are given by the kinematic system (1). The second derivatives M_0 are obtained by the dynamic system (2). The systems of equations (1) and (2) can be represented by:

$$\frac{d\boldsymbol{X}}{d\sigma}(\sigma) = F(\sigma), \quad \boldsymbol{X}(\sigma_0) = \boldsymbol{X}_0, \quad F(\sigma_0) = F_0, \tag{8}$$

where F propagate both kinematic and dynamic systems $\boldsymbol{X}_0$ are the initial values. The numerical solution of this system (8) by the Runge-Kutta method is equivalent to:

$$\boldsymbol{X}(\sigma+\Delta\sigma) = \boldsymbol{X}(\sigma) + \frac{\Delta\sigma}{6}\left[\boldsymbol{H}(\sigma) + 4\,\boldsymbol{H}\left(\sigma+\frac{\Delta\sigma}{2}\right) + \boldsymbol{H}(\sigma+\Delta\sigma)\right]\ , \tag{9}$$

The kinematic ray-tracing gives the ray points coordinates $\boldsymbol{x}_0$ by the adaptive step travel time Runge Kutta method (Cunha, 1999) which control the time step $(\Delta\tau, \Delta s, \Delta\sigma)$ by ray curvature criteria. achieving the magnitude rate of 10^{-6} to the asymptotic relative error when compared with asymptotic analytic solutions by keeping constant in the equations (10) the parameter Δs_p ,

$$\Delta s_p = \frac{\|\Delta\boldsymbol{p}\|}{\|\boldsymbol{p}\|} = \frac{\Delta s}{c^2}\left|\frac{\nabla(1/c)}{(1/c)}\right| = \frac{\Delta s}{\rho} = \Delta\theta = \text{constant}, \tag{10}$$

where ρ is the ray curvature and $\Delta\theta$ is the angle interval between two consecutive slowness vectors. It's easy to see the connection with geometrical optics. The control of time interval control Δs in the interval:

$$\Delta s_{min} \le \Delta s \le \Delta s_{max}\ . \tag{11}$$

The Taylor series expansion decrements the magnitude rate of the relative error by a factor of 10^{-3}.

In order to capture the time of maximum field the algorithm follow the sequence:

1) for each ray point $\boldsymbol{x}_0$ take the slowness $\boldsymbol{p}(\boldsymbol{x}_0)$ from (1), build $M(\boldsymbol{x}_0)$ by first of the equations 7 from informations in equations 2 and build the Taylor series coefficients,

2) determine a square window $\Delta l \times \Delta l$ around the ray point $\boldsymbol{x}_0$ with Δl given by equation 12,

$$\Delta l = {}^{\sigma}\mathcal{J}(\boldsymbol{x}_0)\ /\ c\,\Delta\alpha\ , \tag{12}$$

this guarantees all grid point $\boldsymbol{x}$ to receive contributions from several ray points $\boldsymbol{x}_0$,

3) for each grid point $\boldsymbol{x}$ inside the window calculate:

$$w_t(\boldsymbol{x},\boldsymbol{x}_0) = \frac{{}^{\sigma}\mathcal{J}(\boldsymbol{x}_0)}{\|\boldsymbol{x}-\boldsymbol{x}_0\|^2+\epsilon}\ ,\ \tilde{\tau}(\boldsymbol{x},\boldsymbol{x}_0) = w_t(\boldsymbol{x},\boldsymbol{x}_0)\tau(\boldsymbol{x},\boldsymbol{x}_0), \tag{13}$$

the small parameter ϵ avoid w to be singular and $\tau(\boldsymbol{x},\boldsymbol{x}_0)$ the travel time in the grid point $\boldsymbol{x}$ evaluated by (6) from the ray point $\boldsymbol{x}_0$.

4) accumulate the weight factor $w_t(\boldsymbol{x},\boldsymbol{x}_0)$ in a matrix $W_t(\boldsymbol{x})$ and the weighted time $\tilde{\tau}(\boldsymbol{x})$ in another $T(\boldsymbol{x})$,

$$W_t(\boldsymbol{x}) = W_t(\boldsymbol{x}) + w_t(\boldsymbol{x},\boldsymbol{x}_0), \quad T(\boldsymbol{x}) = T(\boldsymbol{x}) + \tilde{\tau}(\boldsymbol{x},\boldsymbol{x}_0), \tag{14}$$

5) repeat this task for all points of this ray and at final discard all informations off this ray and go to the next,

6) At he final of all rays divide the elements of weighted accumulate matrix $T(\boldsymbol{x})$ by the elements of the total weight matrix $W_t(\boldsymbol{x})$,

$$\tau(\boldsymbol{x}) = \Delta\tau_m + \frac{T(\boldsymbol{x})}{W_t(\boldsymbol{x})} \equiv \frac{1}{W_t(\boldsymbol{x})}\sum_{i=1}^{N(\boldsymbol{x},\boldsymbol{x}_{0_i})} w_t(\boldsymbol{x},\boldsymbol{x}_{0_i})\,\tilde{\tau}(\boldsymbol{x},\boldsymbol{x}_{0_i}), \tag{15}$$

where, $N(\boldsymbol{x},\boldsymbol{x}_{0_i})$ is the total number of ray points $\boldsymbol{x}_{0_i}$ who gives contribution to the grid point $\boldsymbol{x}$ and $\Delta\tau_m$ the time delay from the first arrival to the maximum amplitude travel time of propagating wavelet in the central ray.

Another possibility is to repeat the steps 1-3 and:

4) for each grid point $\boldsymbol{x}$ make a decision:

if $w_t(\boldsymbol{x},\boldsymbol{x}_0) > T(x)$ then $T(x) = \tau(\boldsymbol{x},\boldsymbol{x}_0)$ else endif,

5) repeat the last step (5) until finishing all rays,

6) at the final $T(\boldsymbol{x})$ will have only the contribution for which $w_t(\boldsymbol{x},\boldsymbol{x}_0)$ is maximum.

Amplitude extrapolation

The propagating field $u(\boldsymbol{x})$ in the point $\boldsymbol{x}$ due to point source at $\boldsymbol{x}_s$ can be represented by the integral operator,

$$u(\boldsymbol{x},\boldsymbol{x}_s,t) = \frac{\Re\mathrm{e}}{\pi}\int_{\omega=0}^{\infty} F(\omega)\ G_a(\boldsymbol{x},\boldsymbol{x}_s,w)\ e^{-\imath\,\omega\,t}\,d\omega\ , \tag{16}$$

and as a matter of clarity we will omit in the Jacobean expression the point source coordinate $\boldsymbol{x}_s$ and the asymptotic Green's function for a non homogeneous media can be represented by:

$$G_a(\boldsymbol{x},\omega) = \psi_0(\omega)\frac{e^{\imath\,\omega\tau(\boldsymbol{x})}}{\sqrt{{}^{\sigma}\mathcal{J}(\boldsymbol{x})}}\ , \quad \psi_0(\omega) = \frac{e^{\imath\,\frac{\pi}{4}}}{2\sqrt{2\pi}\sqrt{w}}\ , \tag{17}$$

The Jacobean ${}^{\sigma}\mathcal{J}(\boldsymbol{x})$ by,

$${}^{\sigma}\mathcal{J}(\boldsymbol{x}) = \left|\frac{\partial(x,y)}{\partial(\sigma,\alpha)}\right| = \left|\left[\frac{\partial\boldsymbol{x}}{\partial\sigma},\frac{\partial\boldsymbol{x}}{\partial\alpha}\right]\right| = |[\boldsymbol{p}_\sigma,\boldsymbol{p}_\alpha]|\ . \tag{18}$$

At this point we will be defining $\boldsymbol{x}_0$ and $\boldsymbol{x}$ as ray and grid points respectively. The Jacobean ${}^{\sigma}\mathcal{J}(\boldsymbol{x})$ in a grid point near the ray will be determined from Jacobean ${}^{\sigma}\mathcal{J}(\boldsymbol{x}_0)$ in a ray point by a Taylor's series until its first term,

$${}^{\sigma}\mathcal{J}(\boldsymbol{x}) = {}^{\sigma}\mathcal{J}(\boldsymbol{x}_o) + \left.\frac{\partial^{\sigma}\mathcal{J}(\boldsymbol{x})}{\partial\boldsymbol{x}}\right|_{\boldsymbol{x}_o}\cdot\ (\boldsymbol{x}-\boldsymbol{x}_o) + \mathcal{O}\left(|\boldsymbol{x}-\boldsymbol{x}_o|^2\right)\ . \tag{19}$$

The chain rule to the rectangular coordinates gives:

$$\frac{\partial}{\partial x}=\frac{\partial\sigma}{\partial x}\frac{\partial}{\partial\sigma}+\frac{\partial\alpha}{\partial x}\frac{\partial}{\partial\alpha}\,,\qquad \frac{\partial}{\partial z}=\frac{\partial\sigma}{\partial z}\frac{\partial}{\partial\sigma}+\frac{\partial\alpha}{\partial z}\frac{\partial}{\partial\alpha}\,, \tag{20}$$

applying (20) to the Jacobean:

$$\frac{\partial\,{}^{\sigma}\mathcal{J}}{\partial x}=\frac{\partial\sigma}{\partial x}\frac{\partial}{\partial\sigma}\left|[\boldsymbol{p}_\sigma,\boldsymbol{p}_\alpha]\right|+\frac{\partial\alpha}{\partial x}\frac{\partial}{\partial\alpha}\left|[\boldsymbol{p}_\sigma,\boldsymbol{p}_\alpha]\right|\,, \tag{21}$$

$$\frac{\partial\,{}^{\sigma}\mathcal{J}}{\partial z}=\frac{\partial\sigma}{\partial z}\frac{\partial}{\partial\sigma}\left|[\boldsymbol{p}_\sigma,\boldsymbol{p}_\alpha]\right|+\frac{\partial\alpha}{\partial z}\frac{\partial}{\partial\alpha}\left|[\boldsymbol{p}_\sigma,\boldsymbol{p}_\alpha]\right|\,, \tag{22}$$

assume $\frac{\partial\boldsymbol{x}}{\partial\alpha}$ e $\frac{\partial\boldsymbol{x}}{\partial\sigma}$ exist and are continuous, then:

$$\frac{\partial}{\partial\alpha}\left(\frac{\partial\boldsymbol{x}}{\partial\sigma}\right)=\frac{\partial}{\partial\sigma}\left(\frac{\partial\boldsymbol{x}}{\partial\alpha}\right)\,, \tag{23}$$

It follows,

$$\begin{aligned}
\frac{\partial^{\sigma}\mathcal{J}}{\partial x}&=\frac{\partial\sigma}{\partial x}\left\{\left|\left[\frac{\partial\boldsymbol{p}_\sigma}{\partial\sigma},\boldsymbol{p}_\alpha\right]\right|+\left|\left[\boldsymbol{p}_\sigma,\frac{\partial\boldsymbol{p}_\sigma}{\partial\alpha}\right]\right|\right\}+\\
&\quad\frac{\partial\alpha}{\partial x}\left\{\left|\left[\frac{\partial\boldsymbol{p}_\sigma}{\partial\alpha},\boldsymbol{p}_\alpha\right]\right|+\left|\left[\boldsymbol{p}_\sigma,\frac{\partial\boldsymbol{p}_\alpha}{\partial\alpha}\right]\right|\right\},\\
\frac{\partial^{\sigma}\mathcal{J}}{\partial z}&=\frac{\partial\sigma}{\partial z}\left\{\left|\left[\frac{\partial\boldsymbol{p}_\sigma}{\partial\sigma},\boldsymbol{p}_\alpha\right]\right|+\left|\left[\boldsymbol{p}_\sigma,\frac{\partial\boldsymbol{p}_\sigma}{\partial\alpha}\right]\right|\right\}+\\
&\quad\frac{\partial\alpha}{\partial z}\left\{\left|\left[\frac{\partial\boldsymbol{p}_\sigma}{\partial\alpha},\boldsymbol{p}_\alpha\right]\right|+\left|\left[\boldsymbol{p}_\sigma,\frac{\partial\boldsymbol{p}_\alpha}{\partial\alpha}\right]\right|\right\},
\end{aligned} \tag{24}$$

Considering the equation:

$$\frac{\partial\boldsymbol{p}_\alpha}{\partial\alpha}=\nabla\left[\frac{{}^{s}\mathcal{J}^2}{2}\right]=\nabla\left[\frac{({}^{\sigma}\mathcal{J}c)^2}{2}\right]\,,\quad {}^{s}\mathcal{J}(\boldsymbol{x})=\left|\frac{\partial(x,y)}{\partial(s,\alpha)}\right|\,, \tag{25}$$

For a 2D homogeneous medium with ${}^{s}\mathcal{J}=s=\frac{\sigma}{c}$, and therefore nearby a point source $\boldsymbol{p}_\sigma$ e $\frac{\partial\boldsymbol{p}_\alpha}{\partial\alpha}$ will be parallel to the ray and the last determinant $\left|\left[\boldsymbol{p}_\sigma,\frac{\partial\boldsymbol{p}_\alpha}{\partial\alpha}\right]\right|$, will be null. Given the absence of term $\frac{\partial\boldsymbol{p}_\alpha}{\partial\alpha}$ in differential equations 2, we will assume hereinafter the contribution of the latter determinant $\left|\left[\boldsymbol{p}_\sigma,\frac{\partial\boldsymbol{p}_\alpha}{\partial\alpha}\right]\right|$ as negligible also for non-homogeneous media and will have:

$$\begin{aligned}
\frac{\partial^{\sigma}\mathcal{J}}{\partial x}&=\frac{\partial\sigma}{\partial x}\left\{\frac{dp_{\sigma_x}}{d\sigma}\frac{dz}{d\alpha}-\frac{dp_{\sigma_z}}{d\sigma}\frac{dx}{d\alpha}+\frac{dp_{\sigma_z}}{d\alpha}\frac{dx}{d\sigma}-\right.\\
&\quad\left.\frac{dp_{\sigma_x}}{d\alpha}\frac{dz}{d\sigma}\right\}+\frac{\partial\alpha}{\partial x}\left\{\frac{dp_{\sigma_x}}{d\alpha}\frac{dz}{d\alpha}-\frac{dp_{\sigma_z}}{d\alpha}\frac{dx}{d\alpha}\right\},\\
\frac{\partial^{\sigma}\mathcal{J}}{\partial z}&=\frac{\partial\sigma}{\partial z}\left\{\frac{dp_{\sigma_x}}{d\sigma}\frac{dz}{d\alpha}-\frac{dp_{\sigma_z}}{d\sigma}\frac{dx}{d\alpha}+\frac{dp_{\sigma_z}}{d\alpha}\frac{dx}{d\sigma}-\right.\\
&\quad\left.\frac{dp_{\sigma_x}}{d\alpha}\frac{dz}{d\sigma}\right\}+\frac{\partial\alpha}{\partial z}\left\{\frac{dp_{\sigma_x}}{d\alpha}\frac{dz}{d\alpha}-\frac{dp_{\sigma_z}}{d\alpha}\frac{dx}{d\alpha}\right\}.
\end{aligned} \tag{26}$$

All terms of these equations are available in the kinematic (1) or dynamic (2) systems except for terms $\frac{\partial\sigma}{\partial x}$, $\frac{\partial\theta}{\partial x}$, $\frac{\partial\sigma}{\partial z}$, $\frac{\partial\theta}{\partial z}$ that can be determined by the inverse of matrix $\left[\frac{d\boldsymbol{x}}{d\gamma}\right]$.

In order to capture the maximum field the algorithm follow the sequence:

1) for each ray point $\boldsymbol{x}_0$ calculate the coefficients (26) from informations in the dynamic equations 2 and build the Taylor series (19),

2) determine a square window $\Delta l\times\Delta l$ around the ray point $\boldsymbol{x}_0$ with Δl given by equation 12,

3) for each grid point $\boldsymbol{x}$ inside the window calculate:

$$w_a(\boldsymbol{x},\boldsymbol{x}_0)=\tfrac{1}{\|\boldsymbol{x}-\boldsymbol{x}_0\|^2+\epsilon},\quad {}^{\sigma}\tilde{\mathcal{J}}(\boldsymbol{x},\boldsymbol{x}_0)=w_a(\boldsymbol{x},\boldsymbol{x}_0)\,{}^{\sigma}\mathcal{J}(\boldsymbol{x},\boldsymbol{x}_0), \tag{27}$$

the small parameter ϵ avoid w_a to be singular and ${}^{\sigma}\mathcal{J}(\boldsymbol{x},\boldsymbol{x}_0)$ the Jacobian in the grid point $\boldsymbol{x}$ evaluated by (19) from the ray point $\boldsymbol{x}_0$.

4) accumulate the weight factor w_a in a matrix W_a and the weighted Jacobian ${}^{\sigma}\tilde{\mathcal{J}}$ in another ${}^{\sigma}\mathcal{J}(\boldsymbol{x})$,

$$W_a(\boldsymbol{x})=W_a(\boldsymbol{x})+w_a(\boldsymbol{x},\boldsymbol{x}_0),\quad {}^{\sigma}\mathcal{J}(\boldsymbol{x})={}^{\sigma}\mathcal{J}(\boldsymbol{x})+{}^{\sigma}\tilde{\mathcal{J}}(\boldsymbol{x},\boldsymbol{x}_0), \tag{28}$$

5) repeat this task for all points of this ray and at final discard all informations off this ray and go to the next,

6) At he final of all rays divide the elements of weighted accumulate matrix ${}^{\sigma}\mathcal{J}(\boldsymbol{x})$ by the elements of the total weight matrix $W_a(\boldsymbol{x})$,

$${}^{\sigma}\mathcal{J}(\boldsymbol{x})=\tfrac{{}^{\sigma}\mathcal{J}(\boldsymbol{x})}{W_a(\boldsymbol{x})}\equiv\tfrac{1}{W_a(\boldsymbol{x})}\textstyle\sum_{i=1}^{N(\boldsymbol{x},\boldsymbol{x}_{0_i})}w_a(\boldsymbol{x},\boldsymbol{x}_{0_i})\,{}^{\sigma}\tilde{\mathcal{J}}(\boldsymbol{x},\boldsymbol{x}_{0_i}), \tag{29}$$

Where, $N(\boldsymbol{x},\boldsymbol{x}_{0_i})$ is the total number of ray points $\boldsymbol{x}_{0_i}$ who gives contribution to the grid point $\boldsymbol{x}$.

Another possibility is to repeat the steps 1-3 and:

4) for each grid point $\boldsymbol{x}$ make a decision:

if $w_a(\boldsymbol{x},\boldsymbol{x}_0)>{}^{\sigma}\mathcal{J}(\boldsymbol{x})$ then ${}^{\sigma}\mathcal{J}(\boldsymbol{x})=w_a(\boldsymbol{x},\boldsymbol{x}_0)$ else endif,

5) repeat the last step (5) until finishing all rays,

6) at the final ${}^{\sigma}\mathcal{J}(\boldsymbol{x})$ keeps only the contribution for which $w_a(\boldsymbol{x},\boldsymbol{x}_0)$ is maximum.

7) for each grid point $\boldsymbol{x}$ calculate the asymptotic amplitude:

$$A(\boldsymbol{x})=\frac{\varphi_0}{\sqrt{{}^{\sigma}\mathcal{J}(\boldsymbol{x})}}\,, \tag{30}$$

by substituting (17) in (16) and fixing in the point $\boldsymbol{x}$ the maximum field central ray travel time as: $t_m=\tau(\boldsymbol{x})+\Delta\tau_m$, and $e^{\imath\pi/4}=1/\sqrt{-\imath\omega}$ then,

$$u(\boldsymbol{x},t_m)=\frac{1}{\sqrt{{}^{\sigma}\mathcal{J}}}\frac{\Re\mathrm{e}}{2\pi\sqrt{2\pi}}\int_{\omega=0}^{\infty}\frac{F(\omega)}{\sqrt{-\imath\,\omega}}\;e^{-\imath\,\omega\,\Delta\tau_m}\,d\omega\,, \tag{31}$$

which defines φ_0. The effect of the asymptotic factor $1/\sqrt{\imath\,\omega}$ in the source function shape can be seen in figure 1B. The same effect is observed even in finite difference propagation.

Source function

The source function Fig-1A is defined in time domain by equation 32:

$$f(t)=\left(1-2\pi\,(\,\pi f_c\,(t-T_f))^2\right)\;e^{-\pi(\pi f_c(t-Tf))^2}\,, \tag{32}$$

where, the parameters f_c e T_f determined by,

$$f_c=f_{co}/(3\,\sqrt{\pi})\,,\qquad T_f=2\,\sqrt{\pi}/f_{co}\,, \tag{33}$$

and f_{co} the maximum frequency in the source frequency amplitude (34) spectrum $F(f)$,

$$F(f)=\frac{2\,e^{\left(\imath\,2\pi f T_f-\frac{f^2}{{f_c}^2\pi}\right)}f^2}{{f_c}^3\pi^2},\quad F(\omega)=\frac{4\,e^{\left(\imath\,\omega T_f-\frac{\omega^2}{{\omega_c}^2\pi}\right)}\omega^2}{{\omega_c}^3\pi}. \tag{34}$$

Summary and Conclusions

1. Figure-2 shows the superposition of the snapshot, t = 1.3325 s with the isochrones also of maximum field obtained by the proposed method.
2. Figure-3 shows the effect of applying the phase correction $e^{-\imath/2}$ for caustics in all of the field (see Fig-1B and C). The error decrease in the regions after caustics and increase in the rest.
3. Figure-4 shows the transit times determined by the modified method of Schneider (Faria and Stoffa, 1994), which determines only the first arrivals. It is smooth, does not exhibit problems in the blind zone (regions of low amplitudes and low density of rays), and is fast.

4. Figure-5 shows the superposition of the snapshot, t = 1.3325 s, of the field propagated by finite differences with the isochrone of maximum field, also by finite differences. It can be noticed the perfect capture of the maximum field.
5. Figures-6 A and B show the results for relative errors for times and amplitudes by the proposed method by comparison with the analytical asymptotic solution. We observe an error growth pattern with the central ray distance. However the 10^{-6} scale for times and 10^{-4} for amplitudes demonstrate a very good concordance between the proposed numerical asymptotic solution and the analytical asymptotic solution.
6. Figure-7-A shows the maximum field travel times computed by the finite difference method with $20Hz$ of source frequency. The discontinuities in the time field are associated to the fact the maximum amplitude's field can eventually arrive to the grid point after the first arrival.
7. Figure-7-B shows the travel time field by the method superimposed to the rays. We can observe the the discontinuities between the region of higher amplitudes of the scattering field and the *shadow zone*.
8. Figure-7-C shows the maximum field amplitudes by the finite difference method superposed to the ray trajectory by the proposed method. Through visual inspection we can see a good coherence between the high amplitude regions and the regions of high density of rays.
9. Figure-7-D shows the maximum field amplitudes superposed to the ray trajectory by the proposed method. Through visual inspection we can see a good coherence between the high amplitude regions and the regions of high density of rays.
10. Figure-7-E A shows the relative errors for the times between the method and FDM for $20Hz$. Observe, in the legend that the blue-colored regions correspond to errors above 2%. It is greater in regions near caustics, in regions of great curvature of ray and in points distant from the ray, that is, in little lighted regions also called "shadow zones".
11. Figure-7-F shows the relative errors for the amplitudes for $20Hz$. Observe in the legend that the blue colored regions correspond to errors above 40%. The amplitudes obtained by asymptotic methods are more sensitive than times to the velocity field variations. Such as for the times, the relative errors for the amplitudes are greater in the regions near caustics, in the regions of great curvature of ray and in "shadow zones".
12. Figure-7-G shows the relative errors for the times for $60Hz$ frequency. Observe in the legend that the blue colored regions correspond to errors above 2% as in 7-E. However, the red colored regions are much more abundant. This test confirms that the results for the asymptotic methods are as better as higher the frequency as provided by the theory. From this result we can also conclude that the maximum field times obtained by this method are satisfactory even for this hard test to which they were subject.
13. Figure-7-H shows the relative errors for the amplitudes for the frequency $60Hz$. Observe in the legend that the blue-colored regions correspond to errors above 40% as in figure 7-F. However the red-colored regions are more abundant. Such as for times this test confirms the expected.

References

Aminzadeh, F., Brac, J., and Kuns, T., 1997, 3-d salt and overthrust models: SEG/EAGE.

Cunha, P. E. M., 1999, High precision/fast adaptive step size ray-tracing by curvature criteria: Presented at the 6th Ann. Internat. Mtg., Brazilian Geophysical Society, Soc. Expl. Geophys., Resumos Expandidos, 6o. Congr. Intern. da SBGf.

Cunha, P. E. M., 14-18/sep 2003, 2d/3d paraxial maximum field green's funtion generator: Presented at the 8th Ann. Internat. Mtg., Brazilian Geophysical Society, Soc. Expl. Geophys., Resumos Expandidos, 8o. Congr. Intern. da SBGf.

Faria, E. L., and Stoffa, L. P., 1994, Travel time computation in transversely isotropic media: Geophysics, **59**, 272–281.

Lambaré, G., Lucio, P. S., and Hanyga, A., 1996, Two-dimensional multivalued traveltime and amplitude maps by uniform sampling of ray field: Geophysics, **125**, 584–598.

Popov, M. M., and Pšenčik, I., 1978a, Computation of ray amplitudes in inhomogeneous media with curved interfaces: Studia geophizika et geodetica, **22**, 248–258.

——— 1978b, Ray amplitudes in inhomogeneous media with curved interfaces.: Geofizikalni Sbornic, **24**, 111–129.

Popov, M. M., 1977, On a method of computation of geometrical spreading in an inhomogeneous medium with interfaces.: Doklady Akdemii Nauk (em Russo), **237**, no. 5.

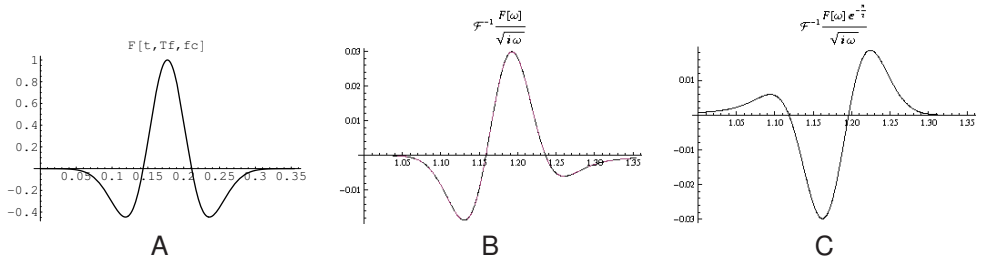

Figure 1: Source function: $f_{co} = 20\,Hz,\ \ T_f = .177\,s,\ \ f_c = 3.76\,Hz,\ \ f_{max} = 6.67\,Hz.$

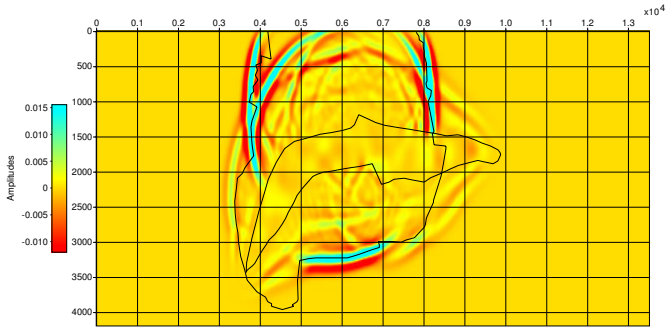

Figure 2: Model SEG/EAGE: MF isochrones by the method

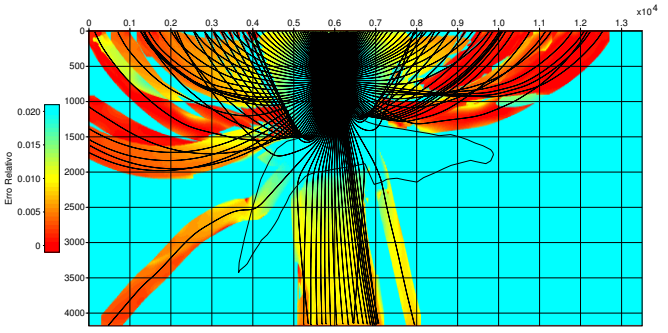

Figure 3: Caustic correction $e^{-\frac{\pi}{2}}$ for SEG model

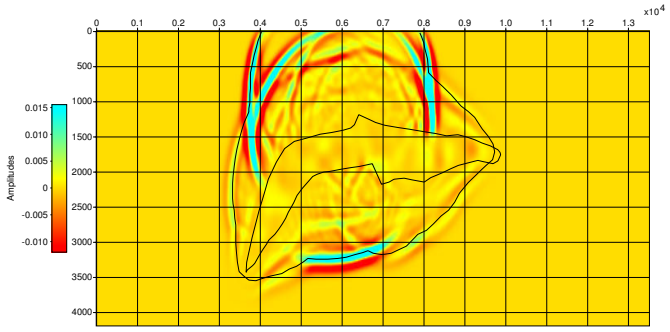

Figure 4: Model SEG/EAGE: isochrones by Schneider

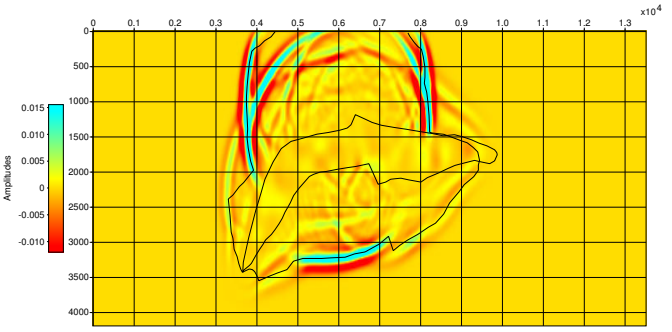

Figure 5: Model SEG/EAGE: snapshot and isochrones by FDM

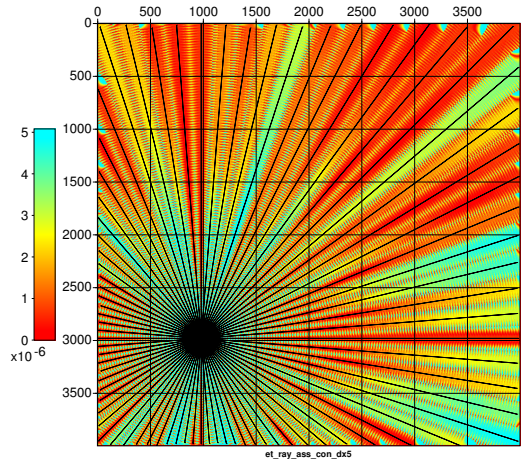

A: Time relative error

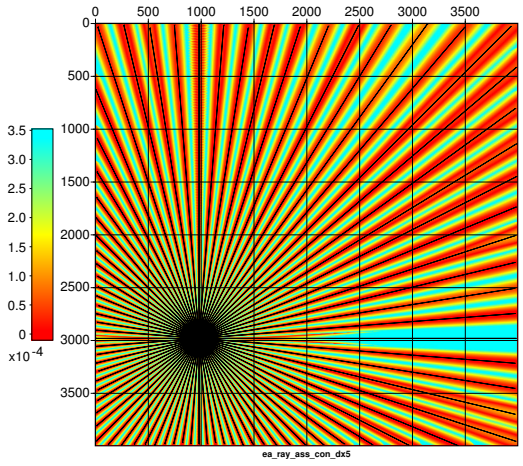

B: Amplitudes relative error

Figure 6: Homogeneous media $f_{co} = 60Hz$ relative errors compared with asymptotic analytic solution.

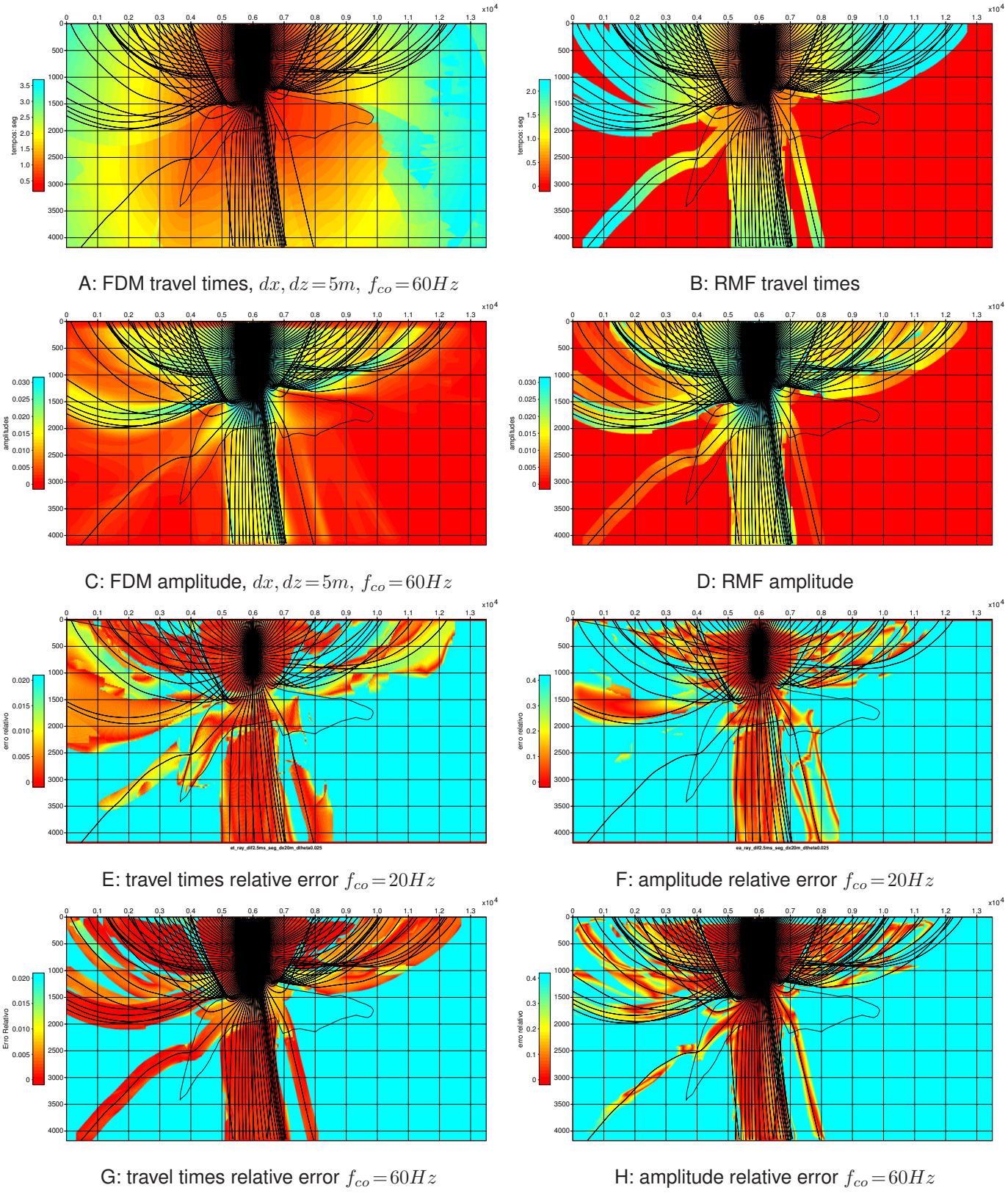

A: FDM travel times, $dx, dz = 5m,\ f_{co} = 60Hz$

B: RMF travel times

C: FDM amplitude, $dx, dz = 5m,\ f_{co} = 60Hz$

D: RMF amplitude

E: travel times relative error $f_{co} = 20Hz$

F: amplitude relative error $f_{co} = 20Hz$

G: travel times relative error $f_{co} = 60Hz$

H: amplitude relative error $f_{co} = 60Hz$

Figure 7: SEG model comparative results with FDM, $(dx, dz = 5m, 20m), \quad f_{co} = 20Hz, 60Hz.$